Nanocomposite-coated porous templates for engineered bone scaffolds: A parametric study of layer-by-layer assembly conditions

To cite this article before publication: Monika Ziminska *et al* 2019 *Biomed. Mater.* in press https://doi.org/10.1088/1748-605X/ab3b7b

Nanocomposite-Coated Porous Templates for Engineered Bone Scaffolds: A Parametric Study of Layer-by-Layer Assembly Conditions

Authors: Monika Ziminska[1], Marine J. Chalanqui[2], Philip Chambers[2], Jonathan Acheson[1], Helen O. McCarthy[2], Nicholas J. Dunne[2,3,4,6], Andrew R. Hamilton[7*]

1. School of Mechanical & Aerospace Engineering, Queen's University Belfast, BT9 5AH, UK

2. School of Mechanical and Manufacturing Engineering, Dublin City University, Dublin, Ireland.

3. Centre for Medical Engineering Research, School of Mechanical and Manufacturing Engineering, Dublin City University, Dublin, Ireland.

4. School of Pharmacy, Queen's University Belfast, 97 Lisburn Road, Belfast BT9 7BL, UK.

5. Trinity Centre for Bioengineering, Trinity Biomedical Sciences Institute, Trinity College Dublin, Dublin, Ireland.

6. Department of Mechanical and Manufacturing Engineering, School of Engineering, Trinity College Dublin, Dublin, Ireland.

7. Engineering and the Environment, University of Southampton, Southampton SO17 1BJ, UK

Abstract

Using the layer-by-layer (LbL) assembly technique to deposit mechanically reinforcing coatings onto porous templates is a route for fabricating engineered bone scaffold materials with a combination of high porosity, strength, and stiffness. LbL assembly involves the sequential deposition of nano- to micro-scale multilayer coatings from aqueous solutions. Here, a design of experiments (DOE) approach was used to evaluate LbL assembly of polyethyleneimine (PEI), polyacrylic acid (PAA), and nanoclay coatings onto open-cell polyurethane foam templates. The thickness of the coatings, and the porosity, elastic modulus and collapse stress of coated foam templates were most strongly affected by the pH of PAA solutions, salt concentration, and interactions between these factors. The mechanical properties of coated foams correlated with the thickness of the coatings, but were also ascribed to changes in the coating properties due to the different assembly conditions. A DOE optimization aimed to balance the trade-off between higher mechanical properties but lower porosity of foam templates with increasing coating thickness. Micromechanical modelling predicted that deposition of 116 QLs would achieve mechanical properties of cancellous bone (>0.05 GPa stiffness and >2 MPa strength) at a suitable porosity of >70%. When capped with a final layer of PAA and cross-linked via thermal treatment, the PEI/PAA/PEI/nanoclay coatings exhibited good indirect cytotoxicity with mesenchymal stem cells. The ability of LbL assembly to deposit a wide range of functional constituents within multilayer-structured coatings makes the general strategy of templated LbL assembly a powerful route for fabricating engineered tissue scaffolds that can be applied onto various porous template materials to achieve a wide range of properties, pore structures, and multifunctionality.

Keywords: porous materials; nanocomposites; coatings; layer-by-layer assembly; bone substitute; tissue scaffolds

1. Introduction

Bone tissue engineering aims to produce patient-specific bone substitutes in an attempt to bypass the limitations of existing clinical treatments (i.e. shortage of donor organs, rejection, disease transfer and cell morbidity [1,2]). A functional engineered bone substitute should exhibit a high level of interconnected porosity that supports tissue and cell in-growth, suitable mechanical properties and structural integrity to temporarily support physiological loadings *in vivo*, and biocompatibility to avoid adverse host responses upon implantation and to promote osteogenesis [3,4]. While there is debate over whether matching the mechanical properties of scaffolds with the host bone tissue is always necessary [3,5], this is a widely accepted target that is particularly important for critical-sized defects in large bones subjected to high levels of mechanical loading [6]. High porosity reduces the amount of load-bearing material and hence the overall mechanical properties, making it difficult to produce scaffold materials with a combination of high mechanical properties and high porosity of greater than 60–70% for native cancellous bone [4,7,8]. This is a key challenge that is yet to be overcome for degradable material systems used in fabricating functional scaffolds for tissue engineered bone grafts.

Layer-by-layer (LbL) assembly is an aqueous-based, template-assisted coating technique that produces conformal multilayer coatings of polymers, inorganic fillers and other constituents (e.g. functional molecules) by the sequential deposition of individual layers with nano-scale precision over thickness [9,10]. LbL assembly typically involves electrostatic attraction and adsorption of oppositely charged electrolytes from aqueous solution onto the template surface. Using LbL assembly to deposit layers of polyethyleneimine (PEI), polyacrylic acid (PAA), and cloisite nanoclay has resulted in coatings with high mechanical stiffness of 15.7 GPa and rapid deposition of ~1 μm per PEI/PAA/PEI/nanoclay quadlayer (QL) [11]. A similar PEI/PAA/PEI/nanoclay material

system has been deposited onto open-cell foam templates, resulting in an increase of compressive elastic modulus from 0.09 to 2.48 MPa with a small reduction in porosity from 98.8 to 96.6% [12]. Coated foams with a range of compressive elastic moduli overlapping those of cancellous bone (50 to 500 MPa [3]) were predicted for coatings with a range of achievable thicknesses and stiffnesses, suggesting that such nanocomposite-coated foams can be tailored to match the stiffness of native bone tissue and applied as engineered tissue scaffolds [12]. PEI and PAA are weak polyelectrolytes that exhibit pH-dependent electrostatic charge densities in aqueous solution [13]. The thickness and mass of PEI/PAA and PEI/nanoclay coatings can be adjusted by changing the pH and salt concentration of the solutions used for LbL assembly because changes in charge density affect polymer chain conformation and diffusion in-and-out of previously deposited layers [10, 14-16]. This in-and-out diffusion of weak polyelectrolytes is associated with more rapid exponential LbL assembly and can help overcome slow rates of deposition, which is a challenge for applications requiring thick films [17]. An increase in contact time with the aqueous solutions can also increase the coating thickness and mass via greater diffusion [18].

Whereas previous work investigated the effect of PEI/PAA/PEI/nanoclay coating thickness on the pore structure and mechanical properties of coated foams [12], this work aimed to study the effects of LbL assembly conditions, including pH, salt concentration, and contact time, on compressive stiffness, strength, and pore structure of PEI/PAA/PEI/nanoclay coated foams. A design of experiments (DOE) methodology was used to assess the significant factors affecting key scaffold properties, and to select optimum assembly conditions for coated foams with targeted combinations of porosity, stiffness, and strength. As an essential step for biomedical applications, the indirect effect of coated foams on cellular response [19] was determined through *in vitro* cytotoxicity analysis, and improved by engineering the surface of the multilayer coatings.

2. Materials & Methods

2.1. Materials

Aqueous solutions of 35 wt% PAA (MW 100 kDa), and 50 wt% PEI (MW 750 kDa) were purchased from Sigma Aldrich, UK. Cloisite Na+ nanoclay was provided by BYK Additives Ltd., USA. Solutions of 1 wt% PEI and PAA were prepared by dilution in deionised (DI) water under vigorous stirring for 12 h. The pH of PEI was either unchanged at approximately 10.5 or adjusted to 8.75 or 7 by adding 0.1 M HCl. The pH of PAA was adjusted to 4, 6 or 8 by adding 0.1 M NaOH. Salt concentrations of 0.5 M and 1 M were prepared by dissolving medical grade NaCl in DI water before addition of the polymer solution. A solution of 0.5 wt% nanoclay was prepared by vigorous stirring the nanoclay in DI water for 24 h, and with pH unchanged at approximately 10–10.5.

An open-cell polyurethane (PU) foam with 30 pores per inch (PPI) and a pore volume fraction of approximately 98% was used as the template for LbL assembly (The Foam Shop Ltd, UK). This foam template material was selected for its biocompatibility and consistent porous architecture that is similar to cancellous bone, as evidenced by its use as a substrate for the evaluation of orthopedic devices and cancellous core material in bone models [20,21]. Cylindrical specimens (12.7 mm in diameter and 10 mm in height) were cut from the foam using a punch stamp (Figure 1a and Figure 1b). Glass coverslips (13 mm diameter) were purchased from Agar Scientific, UK.

2.2 LbL assembly of Coating

Specimens for physico-mechanical characterization

LbL assembly of conformal coatings onto PU foam templates was conducted in a deposition chamber, through which the alternating flow of electrolyte solutions was controlled using a computer-controlled system of solenoid valves. Before deposition, foam templates were cleaned in 1 M NaOH solution for 10 min, repeatedly rinsed with DI water, and dried for 24 h. Foams were placed in the deposition chamber, which was filled with alternating solutions of the polycationic PEI, polyanionic PAA, PEI, and anionic nanoclay. Different levels of pH and salt concentrations were used for PEI and PAA solutions, depending on the experimental run. The contact time of the template in each solution was either 30 s, 65 s, or 100 s. The introduction of each solution was punctuated by three rinses in DI water, each with a total contact time of 30 s. This sequence (shown in Figure 1c) resulted in the deposition of one quadlayer (QL) of PEI/PAA/PEI/nanoclay coating. The full PEI/PAA/PEI/nanoclay deposition cycle was repeated 5, 10, or 15 times, resulting in the deposition of a 5, 10, or 15 QL coating after which coated foams were rinsed three times in DI water and dried for 24 h under ambient conditions (approximately 23°C and 30% relative humidity). This process was repeated to deposit additional layers up to a total of 60 QLs. To investigate the effect of cyclical mechanical deformation on the coating deposition rate, specified foam templates were subjected to a compressive strain amplitude of 5% at a frequency of 1 Hz using a custom computer-controlled linear motor and plunger situated within the deposition chamber.

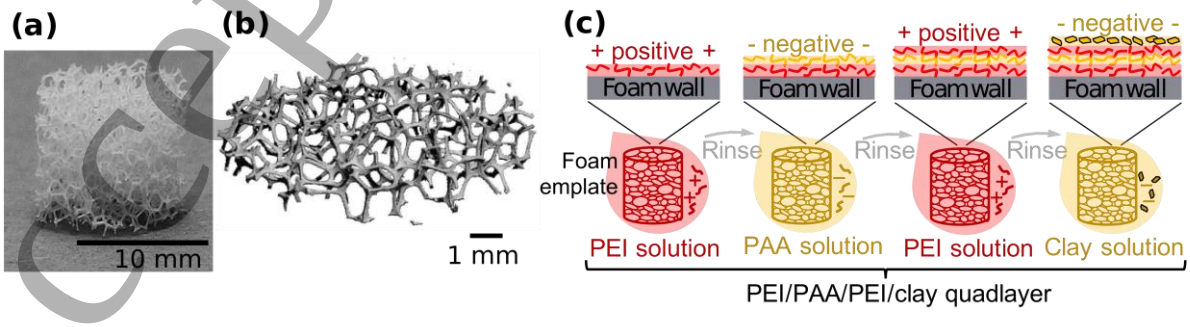

Figure 1. (a) PU foam template, (b) volumetric reconstruction of a 1 mm tall cross-section from a PU foam template, (c) LbL assembly sequence for depositing a single PEI/PAA/PEI/nanoclay QL onto a foam template, with schematics (top) depicting the coating multilayer structure.

Specimens for cytotoxicity testing

Foam templates were coated with 10 PEI/PAA/PEI/nanoclay QLs assembled using the conditions identified as optimum by the DOE analysis in Section 3.2 (PEI pH 7.69, PAA pH 4, 30 s solution contact time and with 1 mm total deformation), and using the process parameters that resulted in the thinnest coatings (PEI 10.5, PAA 8, and 30 s solution contact time). A final capping layer of PAA was deposited by rinsing coated substrates in DI water, immersing them into a solution of PAA, and repeating this three. Thermally treated PAA capping layers were placed in a furnace (Elite Thermal Systems Ltd, UK) at 180°C for 60 min to induce thermal cross-linking of PEI/PAA [22]. Before cell seeding, each foam template was sterilized in an Ultra-Lum UVA-10 Ultraviolet Light Box (wavenumber of 365 nm) at the maximum intensity for 2,000 min.

2.3 Experimental design

A two-level ½ fractional factorial DOE [23] was developed using Design-Expert V8 software (Stat-Ease Inc, USA). The DOE included six variables (or factors), each at a lower and upper level (Table 1). The selected PAA pH levels (factor A) represented values at which the polymer is weakly charged (pH 4) and almost fully charged (pH 8). Similarly, the PEI pH levels (factor B) correspond to a weakly charged (pH 10.5) and highly charged state (pH 7). Highly charged polyelectrolytes have a flattened conformation that has been associated with thinner, denser films, whereas weakly charged polymers have a coiled conformation leading to relatively thick films [18]. Drying steps (factor C) were included every five QLs based on previously reported conditions for

PEI/PAA/PEI/nanoclay coated foams [12], and an upper level of 15 QLs was investigated as a means to reduce the total processing time. Solution contact time with the templates (factor D) of 30 s and greater were investigated due to the anticipated increase in coating thickness and corresponding increase in foam mechanical properties. No salt (0 M NaCl) was used as the lower level of salt concentration (factor E), and a relatively high concentration of 1 M NaCl was used as the upper level to assess its influence on exponential growth and the deposition rate (expected at > 0.15 M [13,24]), and on the mechanical properties of the coatings (expected at approximately 1 M [25]).

Table 1. Two level design of experiment input factors for PEI/PAA/PEI/nanoclay LbL assembly.

Factor	Parameter	Units	Lower level	Upper level
A	PAA pH	-	7	10.5
B	PEI pH	-	4	8
C	Frequency of drying	QL	5	15
D	Contact time	s	30	100
E	Salt concentration	M	0	1
F	Deformation	-	No	Yes

The effect of cyclic mechanical deformation (applied during LbL assembly) on the physical and mechanical properties of polymer-nanocomposite coatings was also investigated (factor F). Cyclic loading has been reported to affect diffusion rates and enhance solute transport of large molecules into hydrated gels [26] with similar structure and properties to exponentially grown LbL-assembled material systems [27]. Mechanical stretching has also been reported to reversibly open nanopores in LbL-assembled PDADMA/PSS films that act as diffusion barriers [28]. Applying cyclic mechanical loading during LbL assembly could therefore increase the rate of in-and-out diffusion of polyelectrolytes and increase the thickness of the coatings, with the potential for localization of thicker QL coatings in regions of higher mechanical loading.

The experimental design did not include replication runs, therefore six replication center points were incorporated (PAA pH 6, PEI pH 8.5, drying frequency of 10 QL, contact time 65 s, salt concentration 0.5 M, three specimens each with/without cyclic deformation). The replication points allowed for an independent estimate of error and calculation of model curvature [29]. One experimental run was conducted for each of the 38 conditions (2^{6-1} + 6) [30]. The full set of

experimental conditions specified in the fractional factorial DOE are provided in Table S1. Each experimental run was randomly assigned and performed in the assigned run order. The physico-mechanical properties analyzed as outputs of the DOE were thickness per QL and mass per QL of coatings, as well as porosity, compressive elastic modulus, and collapse stress of the coated foam templates. The optimal process parameters were determined using goals of highest elastic modulus, collapse stress, and porosity, and lowest thickness and mass per QL. The goals define a desirability objective function that is maximized by a numerical optimization algorithm in the Design-Expert software.

2.4 Physico-mechanical characterization

Coating thickness and porosity

Volumetric imaging was performed using a μCT40 X-ray micro-focus computed tomography (microCT) system (Scanco Medical, Switzerland) at a nominal resolution of 16 μm. Microstructural analysis was performed on reconstructed image slices segmented at an intensity of 20 after applying a Gaussian filter with a standard deviation of 0.8 over a window including each neighboring pixel (support of 1). The strut thickness and porosity of uncoated foam templates (n = 5) was characterized to obtain a baseline for comparison with the 60 QL coated foams. The coating thickness was calculated as the difference between the mean trabecular thickness (Tb.Th) of the coated foam and the mean Tb.Th averaged over the five uncoated foam templates. Tb.Th was measured using a sphere-fitting method, where thickness was calculated as the maximum sphere diameter that could be placed inside the strut [31]. The total coating thickness was divided by the number of QLs (i.e. 60) to obtain thickness per QL.

Coating mass

Each uncoated and coated foam template was weighed using an analytical balance (accurate to 1 mg) following drying (as specified by factor C) for a minimum of 8 h under ambient conditions (approximately 23°C and 30% relative humidity). The coating mass was calculated as the difference between the mass of the coated and uncoated PU foam templates. The total coating mass was divided by the number of QLs (i.e. 60) to obtain mass per QL.

Compressive mechanical behavior

Quasi-static mechanical testing in compression was conducted using a Lloyds LRX materials testing machine (Lloyds Instruments, USA) with a 50 N load cell following ASTM D1621-10 [32] with non-standard specimen dimensions (12.7 mm diameter and 10 mm height). Specimens were deformed at a rate of 2 mm/min starting from a preload of 0.03 N to a final displacement of 6 mm (60% nominal strain). The compressive elastic modulus was calculated as the slope of the stress-strain curve in the linear region. The collapse stress was determined as the maximum stress following the elastic region.

Statistical analysis

Statistical analysis of the experimental data was conducted to assess the significance of the LbL assembly process parameters. Half-normal probability plots, analysis of variance (ANOVA) tables and effect plots were used to identify the contributing parameters and interactions that significantly affected the different physico-mechanical outputs (significance assessed as p value of < 0.05). Factors or interactions of factors with a significant effect on an output response were ranked in order of p value. An effect above 10% contribution to a specific output response was deemed significant [33]. The experimental results for coating thickness and mass per QL, porosity and compressive elastic modulus all exhibited a normal distribution. A square root distribution

transformation was applied to collapse stress data, which was not normally distributed, to better fit the data to the model.

2.5 Cytotoxicity characterization

Porcine bone marrow mesenchymal stem cells (pBM-MSCs) were isolated from the bone marrow of adult pig femora (AFBI, UK). The pBM-MSCs were cultured in Dulbecco's modified essential medium (DMEM) with Glutamax™ supplement, 10% fetal bovine serum (FBS) and 1% antibiotic mixture (Gibco, UK). The pBM-MSCs were incubated at 37°C in an atmosphere of 5% CO_2 and a humidified environment. The cell medium was changed twice weekly, and cells were dissociated using 0.5% Trypsin-EDTA (Gibco, UK) at qualitative confluency and were used at passages 3–5. Cell viability was assessed using the CellTiter 96® Aqueous One Solution Cell Proliferation Assay (MTS reagent, supplied by Promega, UK). pBM-MSCs were counted using a hemocytometer and cell viability was assessed by a dye exclusion test [34].

Uncoated and coated foam templates were submerged in 1 mL Opti-MEM reduced serum medium (Gibco, UK) and incubated for 1, 3, 7 and 14 days in a humidified atmosphere with 5% CO_2 at 37 °C. At each time point, 100 µL of medium was extracted from each well and stored at 4°C until transfection. 10 x 10^3 pBM-MSCs were seeded in a 96-well plate with 100 µL of fresh DMEM reduced serum media and incubated under standard culture conditions for 24 h. The DMEM medium was then replenished with 100 µL of Opti-MEM medium and incubated for a further 2 h, followed by removal of the Opti-MEM medium and addition of 100 µL of the foam extraction medium (removed after 1, 3, 7 or 14 days). For the untreated control group, fresh Opti-MEM medium was added instead of extraction medium. Cells were incubated with 5% CO_2 at 37°C for 24 h before 120 µL of MTS solution was added per well and incubated for 2 h at 37°C to

assess viability. Cytotoxicity tests were repeated three times (n = 3) for each material and for each time point.

For each test, absorbance was recorded at 490 nm with a FLUOstar Omega plate reader (BMG LABTECH®), and the number of living cells calculated as directly proportional to the quantity of formazan product. Phase-contrast images of pBM-MSC cells in supernatant were captured using an EVOS FL microscope (Life Technologies) after cell culture for 24 h in an extract medium that was incubated for 14 days with coated and uncoated foam templates.

3. Results and Discussion

Unocated PU foam templates exhibited an average porosity of 97.4 ± 0.1%, strut thickness of 84.7 ± 1.90 μm, pore size of 973 ± 6 μm and connectivity density of 1.21 ± 0.26 mm^{-3}. The deposition of nanocomposite coatings onto the PU foam templates increased the strut thickness, mass, compressive elastic modulus, and collapse stress, and decreased the porosity (Table S2). The pH of the PAA solution (factor A) and salt concentration (factor E) were dominant factors for all output responses, with combined contributions ranging from 45%–78% across all output responses (Table 2). Any potential effect of the other factors was difficult to assess based on the low contributions relative to factors A and E. Contact times (factor D) of 30 s and 2 min (similar to the levels in this study) have been previously reported to almost double the thickness of similar PEI/PAA/PEI/nanoclay material systems [11], but any potential effect in this study was masked by the more dominant factors A and E. These dominant factors also masked any potential effect of cyclic mechanical deformation (factor F) as a possible parameter affecting LbL assembly, and thus this study was inconclusive about the hypothesized effect on in-and-out diffusion and QL thickness.

Table 2. Parameters and significant interactions between the LbL assembly conditions that contributed to changes in the characteristics of coated PU foam templates.

Factor/Interaction	Parameter	% Contribution				
		Thickness/QL	Mass/QL	Porosity	Elastic modulus	Collapse stress
A	PAA pH	18.64	17.70	15.13	14.23	12.94
B	PEI pH	2.02	2.28	0.01	0.30	2.11
C	Frequency of drying	1.88	0.04	2.40	2.46	0.75
D	Contact time	1.62	3.01	5.68	1.16	3.70
E	Salt concentration	13.96	25.16	16.55	48.31	30.03
F	Deformation	1.46	0.02	0.87	1.32	0.83
AB		12.3	10.02	9.24	1.27	10.72
AE		14.27	15.23	13.74	15.46	15.30
BE		10.16	7.00	7.65	0.03	7.07
ABE		11.73	10.44	9.68	2.13	8.83
Sum of other interactions		11.96	9.11	19.05	13.33	7.72
Total		100	100	100	100	100

3.1 Physico-mechanical properties

Coating thickness

Before coating deposition, the average strut thickness of PU foam templates was 84.7 ± 1.90 μm. The increase in strut thickness per QL after deposition of a 60 QL coating ranged from 0.12 to

3.28 μm/QL (Figure 2a). The pH of PAA solution exhibited the highest contribution to thickness per QL (18.64% in Table 2). At weakly charged PEI (pH 10.5), changing from weakly to strongly charged PAA (increasing pH from 4 to 8) resulted in a 79.9 % decrease in thickness per QL (Figure 2b). At strongly charged PEI (pH 7), this effect of PAA charge was reduced, and resulted in 50.3% thinner coatings when PAA was weakly charged (pH 4). At 0 M NaCl, increasing the charge density of PAA (pH 4 to 8) resulted in a 73.2% decrease in thickness per QL (Figure 2c), but increasing salt concentration to 1 M NaCl reduced this effect and resulted in 67.8% thinner coatings at PAA pH 4 (weak charge). With strongly charged PEI (pH 7), salt concentration had little effect on thickness (Figure 2d), but with weakly charged PEI (pH 10.5) thickness per QL was 74.1% lower in the presence of 1 M NaCl. As shown on the cubic interaction plot between PAA pH, PEI pH, and salt concentration (Figure 2e), the lowest thickness of 0.28 μm per QL was obtained for PEI pH 10.5, PAA pH 8, and no salt, which was similar to previous reports (i.e. 0.25 ± 0.09 μm per QL at PEI pH 10.5, PAA pH 8, and 0 NaCl) [12].

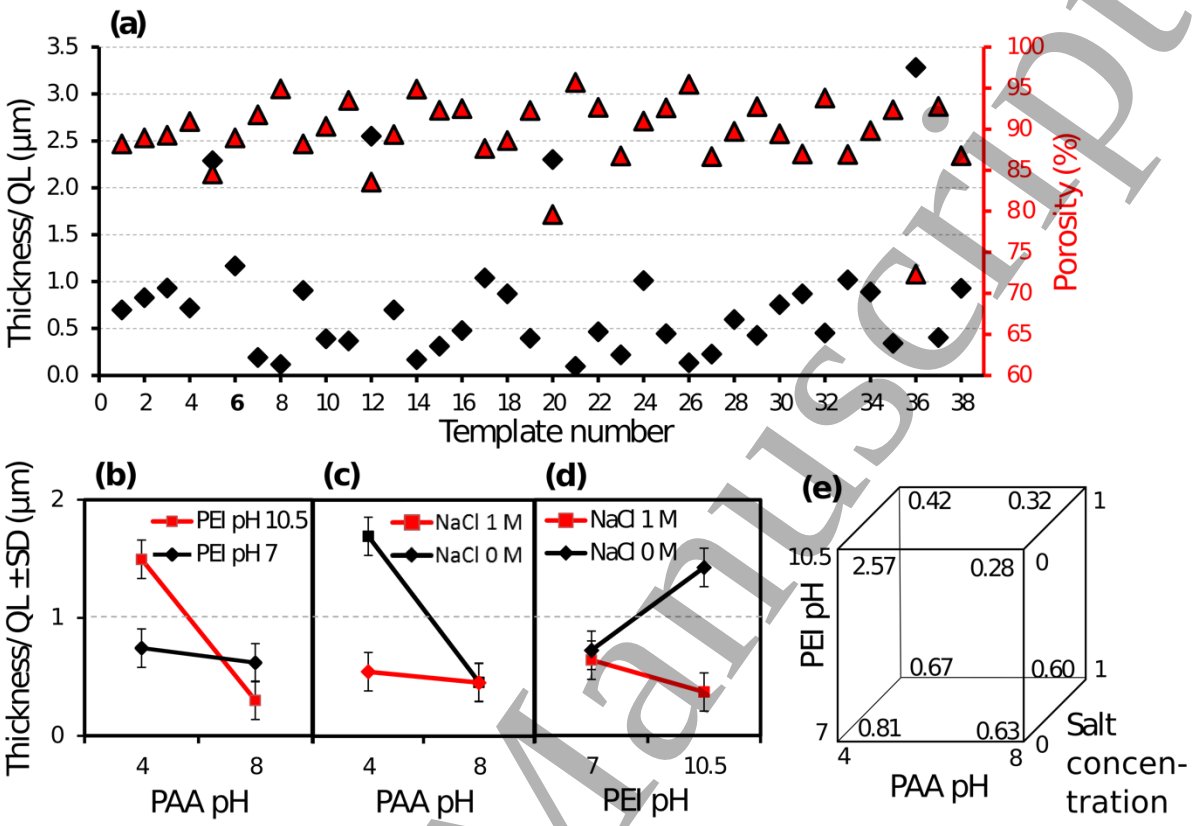

Figure 2. Response of coating thickness per QL. (a) Coating thickness per QL and porosity for each experimental run. Interactions between (b) PAA pH and PEI pH (AB), (c) PAA pH and salt concentration (AE), (d) PEI pH and salt concentration (BE), and (e) PAA pH, PEI pH and salt concentration (ABE) when other conditions (factors C, D, F) were constant.

The significant contributions of PAA pH, salt concentration, and interactions with PEI pH were consistent with reports that pH and ionic strength affect the properties of LbL-assembled PEI/PAA films by changing polymer chain conformation and degree of physical entanglement [35,36]. Relatively thicker PEI/PAA films (0.16 µm per bilayer) have been reported for weakly charged PEI and PAA (pH 10 and 4, respectively), and relatively thinner films (0.003 µm per bilayer) for higher charge densities (both at pH 7) [37]. Similarly, in this study the thickest coatings (2.57 µm per QL) were obtained with weakly charged PEI (pH 10.5) and PAA (pH 4), and highly charged PEI

(pH 7) and PAA (pH 8) produced thinner coatings (0.63 μm per QL), as in Figure 2e. This was consistent with strongly charged polymers assuming flattened conformations due to self-repulsion, and weakly charged polymers assuming coiled conformations [37]. In addition, weakly charged PEI and PAA can enhance the in-and-out diffusion of free polyelectrolytes that is associated with rapid exponential growth of nanocomposite coatings [17]. Coatings assembled in the presence of salt exhibited similar or lower thickness compared to coatings without salt, consistent with reports for polyallylamine hydrochloride/PAA films [38]. Although salt promotes coiling by shielding self-repulsion it has been reported to suppress the electrostatic attractions between polyelectrolytes leading to reduced film deposition [39]. The effect of salt on coating thickness was relatively small when either solution had a high charge density, suggesting that the flattened conformation of the highly charged polymer was dominant over the tendency for salt counter-ions to promote polymer coiling [40].

Coating mass

Prior to coating deposition, the average mass of the foam templates was 35.2 ± 0.70 mg. The increase in mass per QL of coatings ranged from 0.23 to 8.62 mg/QL (Figure 3a). As with thickness, the coating mass was predominantly affected by the pH of PAA and salt concentration. Changing PAA from weakly to highly charged (pH 4 to 8) when PEI was weakly charged (pH 10.5) reduced the coating mass by 80.1% (Figure 3b); similar to the 79.9% reduction in coating thickness for the same assembly conditions (Figure 2b). When PAA was highly charged (pH 8), the films did not exhibit a significant difference in coating mass irrespective of PEI pH (Figure 3b). A similarly large decrease in mass per QL occurred when increasing PAA charge density with 0 M NaCl (Figure 3c), but 1 M NaCl reduced the mass per QL and the effect of PAA pH. Mjahed, *et al*. also observed that an NaCl concentration above 0.37 M decreased the coating thickness and

mass of polyelectrolyte films [25]. Increasing the pH (and charge) of PAA decreased the mass per QL, but this effect was suppressed with highly charged PEI (pH 7) and at a higher salt concentration of 1 M (Figure 3d), which is analogous to the trends observed for coating thickness. All coatings assembled in the presence of salt exhibited lower mass per QL. Interestingly, at PEI pH 10.5 and PAA pH 8, the mass per QL decreased (from 0.83 to 0.62 mg) upon addition of salt, whereas the thickness per QL increased (from 0.28 to 0.32 μm). This apparent decrease in density could be the result of swelling due to salt ions [13,24], resulting in a less dense coating upon drying.

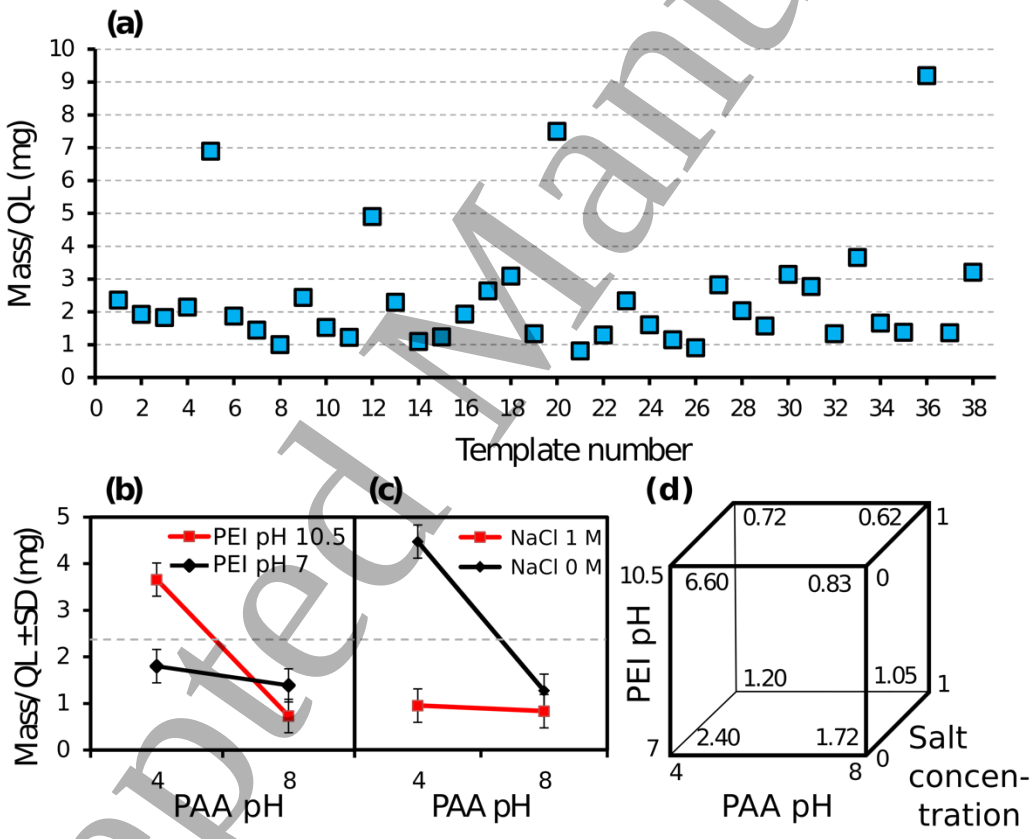

Figure 3. Response of the coating mass per QL. (a) Coating mass per QL for each experimental run. Interactions between (b) PAA pH and PEI pH (AB), (c) PAA pH and salt concentration (AE), (d) PAA pH, PEI pH and salt concentration (ABE) when other conditions (factors C, D, F) were constant.

Porosity

Before coating deposition, the average porosity of foam templates was 97.4 ± 0.1%, which decreased to between 72.3–95.2% following deposition of 60 QL coatings (Figure 2a). Coating deposition decreased porosity because pore space was occupied by the coating material. Similar to coating thickness and mass, PAA pH and salt concentration were the dominant contributing factors affecting porosity. Salt concentration and PAA pH had the opposite effect on porosity compared to coating thickness and mass. Porosity was 4.3% higher for highly charged PAA (pH 8), and 4.5% higher in the presence of 1 M NaCl because thinner coatings occupied less pore space (Figure 4a). High salt concentration suppressed the effect of PAA pH and strongly charged PAA (pH 8) suppressed the effect of salt (Figure 4a). The high porosity and low strut thickness of foam templates coated with highly charged PAA (pH 8) is shown in Figure 4b (porosity 93.8%). The small effect of increasing salt concentration at PAA pH 8 is apparent in Figure 4c (porosity 95.7%). However, with PAA at low charge density (pH 4), the porosity increased from 84.6% at 0 M salt (Figure 4d) to 95.5% at 1 M salt (Figure 4e). For all experimental runs, the porosity remained above the minimum requirement of 60% for cancellous bone substitutes, and so additional coating layers could be deposited to achieve other targeted properties (e.g. mechanical behavior) without exceeding this minimum porosity. The porosity could also be further reduced and adjusted to match specific anatomical site requirements by adjusting the QL number deposited or varying the pH of the PAA and PEI solutions.

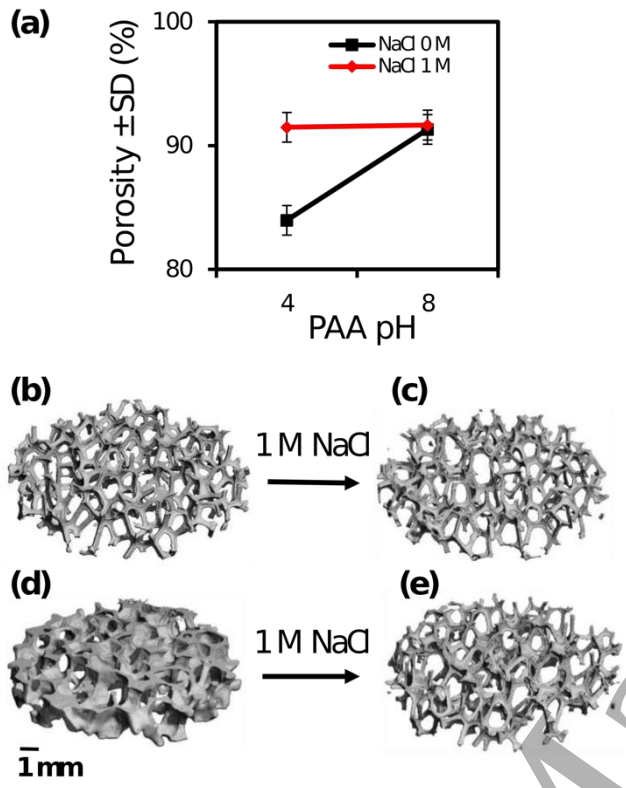

Figure 4. Response of the porosity of coated foams. (a) Interaction between PAA pH and salt concentration (AE) when all other input variables were held constant. Volumetric reconstructions of 60 QL coated foams illustrating the effect of (b) 0 M NaCl and (c) 1 M NaCl with highly charged PAA (pH 8), and (d) 0 M NaCl and (e) 1 M NaCl with weakly charged PAA (pH 4); in all cases PEI was weakly charged (pH 10.5) and other conditions (factors C, D, F) were constant.

Compressive elastic modulus

Prior to coating deposition, the foam templates exhibited an average compressive elastic modulus of 0.08 ± 0.01 MPa, which increased to between 0.32 and 16.64 MPa following deposition of a 60 QL coating. The elastic modulus of coated foam templates is shown as a function of porosity in Figure 5a. As with coating thickness, mass, and porosity, the modulus was affected predominantly by PAA pH, salt concentration, and the interaction between these two parameters

(Table 2). At 0 M NaCl, changing PAA charge density from low to high (pH 4 to 8) decreased the elastic modulus by 57.0% (Figure 5b), which corresponded to a 73.2% drop in coating thickness (Figure 2c) and 78.7% reduction in coating mass (Figure 3c). When foam templates were coated in the presence of 1 M NaCl, the elastic modulus did not change appreciably with an increase of PAA pH, similar to the trends observed for coating thickness (Figure 2c) and mass (Figure 3c). For most assembly conditions, the elastic modulus followed the same trends as coating thickness, mass and porosity. However, for highly charged PAA (pH 8), the elastic modulus of coated foams decreased by 75.0% on addition of 1 M NaCl (Figure 5b), whereas there was no appreciable effect on coating thickness and mass (Figures 2b and 3c). This decrease in elastic modulus was consistent with changes in the mechanical properties of the coating, which can be attributed to the interference of ionic cross-links between carboxyl group of PAA and amine group of PEI in the presence of salt [24]. Increasing salt concentration from 0 to 1 M has been reported to reduce the adhesive force between multilayers (from 2.9 to 1.9 nN), resulting in a softer polyelectrolyte multilayer coating [25]. Changes in mechanical properties of the coating may also be due to possible differences in the nanoclay content of coatings deposited under different process conditions, which was not characterized in this study, but has been reported as 39–45 wt% in similar coating materials [41].

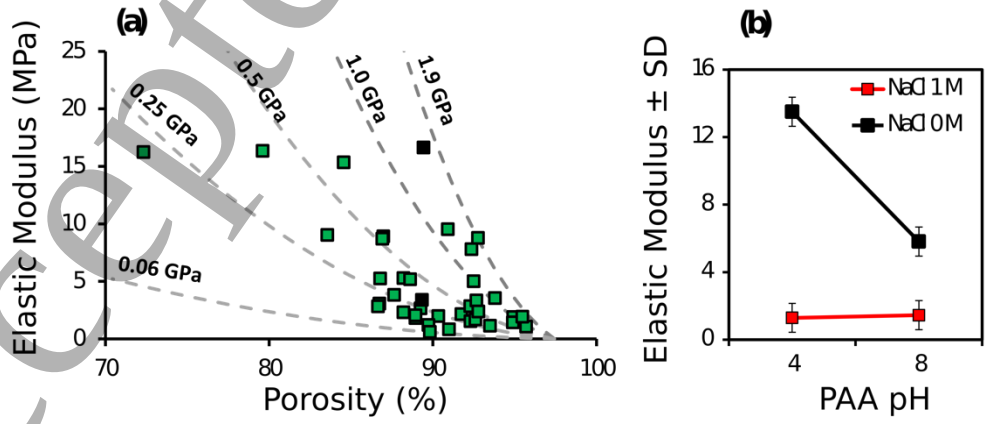

Figure 5. Response of the compressive elastic modulus of coated foams. (a) Elastic modulus of coated foam templates as a function of porosity with predicted trends (dashed lines) assuming elastic modulus of the coating, E_c = 0.06 – 1.9 GPa. (b) Effect of interaction between PAA pH and salt concentration (AE) on foam compressive elastic modulus with all other input variables constant.

Micromechanical models for cellular materials predict the compressive elastic modulus of open-cell foams as $E^* = CE_b(t/l)^4$, where $C \approx 1$ is a constant related to the unit cell geometry, l is the edge length and t is the strut thickness of an open unit cell, and E_b is the effective modulus of the strut in bending [42]. For a coated foam template, $E_b = [E_o t_o^4 + E_c(t_c^4 - t_o^4)]/(t_c^4)$, where t_o is the uncoated strut thickness, E_o is the elastic modulus of the uncoated strut material, t_c is the thickness of a coated strut, and E_c is the elastic modulus of the coating [43]. Thus, expressing the modulus of a coated foam template as a function of porosity, $\phi = 1 - (t/l)^2$, yields:

$$E^* = (1-\phi_o)^2(E_o - E_c) + (1-\phi_c)^2(E_c), \quad \text{Equation (1)}$$

where the porosity of the uncoated (ϕ_o= 97.4 ± 0.1%, with t = 84.7 ± 1.90 μm) and coated (ϕ_c) foam templates were measured by microCT, and the elastic modulus of the PU uncoated foam strut material was taken as E_o= 0.5 MPa [44]. The predicted trend lines in Figure 5a were plotted assuming the elastic moduli of the coating ranged from E_o= 0.06 to 1.90 GPa. These trend lines delineate the coatings with higher apparent elastic moduli, which can be attributed to structural changes in the coatings resulting from variations in the processing conditions. Such changes enable a means of tailoring the mechanical properties of coated foam templates independent of porosity.

Collapse stress

Prior to coating deposition, the foam templates exhibited an average collapse stress of 4.46 ± 0.42 kPa, which increased to 64–3950 kPa following deposition of a 60 QL coating (Figure 6a). A square root transformation resulted in the best fit based on Box-Cox and λ value analysis, and so the effect graphs are presented as the square root of the collapse stress (σ½). The collapse stress was predominantly affected by the salt concentration, which contributed to 30% of the response output, compared to 48.3% for the elastic modulus. The influence of PAA pH, salt concentration, and interactions between these and PEI pH concur with previous trends. Changing the PAA charge density from low to high (pH 4 to 8) and addition of 1 M NaCl reduced the collapse stress (Figure 6b and Figure 6c). When coatings were assembled with highly charged PEI (pH 7) or 1 M NaCl salt concentration, the collapse stress was lower and changing the charge density of PAA had a smaller effect. For highly charged PAA (pH 8), the collapse stress changed little when the pH of the PEI solution or the salt concentration were changed. Predicted trend lines in Figure 6a were plotted based on micromechanical modelling of open-cell foams that predicts collapse stress (σ_c^*) is proportional to elastic modulus, $\sigma_c^* = 0.05E^*$, and using Equation 1 with coated elastic moduli ranging from E_o = 0.06 to 1.90 GPa. As with elastic modulus (Figure 5a), these trend lines delineate coatings with higher apparent elastic moduli. These differences can be attributed to structural changes in the coatings and could be exploited to tailor strength independent of porosity by processing parameter adjustment.

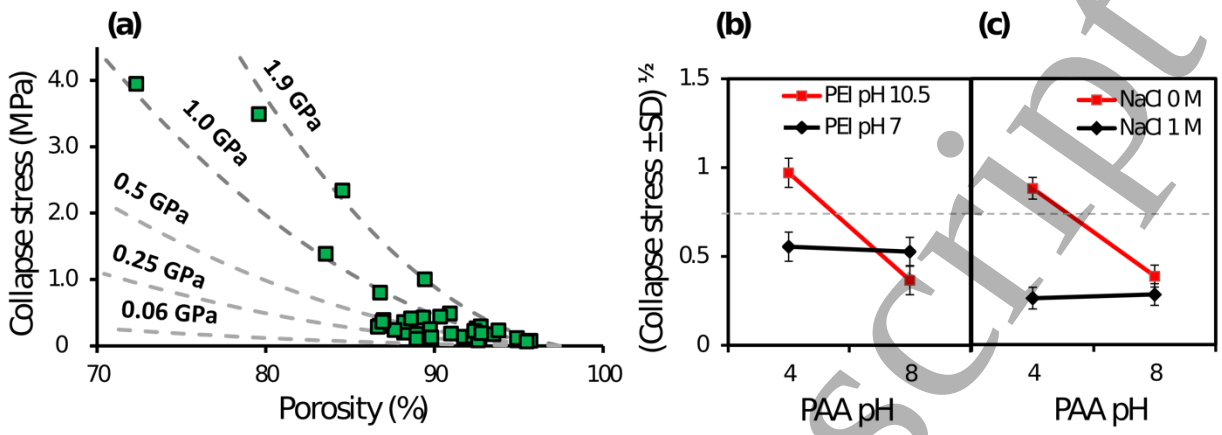

Figure 6. Response of the collapse stress of coated foams. (a) Collapse stress of coated foam templates as a function of porosity with predicted trends (dashed lines) assuming values of elastic modulus for the coating, E_c = 0.06 – 1.9 GPa. Effect of interactions between (b) PAA pH and PEI pH (AB), and (c) PAA pH and salt concentration (AE) on collapse stress when all other input variables were constant.

Process Optimization

The optimization of processing parameters aimed to balance the trade-off between high mechanical properties, and high porosity (low coating thickness and mass) of 60 QL coatings. The optimal conditions were determined as weakly charged PAA of pH 4, highly charged PEI pH of 7.69, 0 M NaCl, drying steps every 10 QLs, 30 s solution contact time, and with cyclic mechanical deformation applied. This optimization is consistent with the relatively higher mechanical properties and intermediate porosity observed at PAA pH 4 and 0 M NaCl. The properties of the coated foam templates assembled under optimized processing conditions were measured and compared to the DOE predictions (Table 3). Measured values were within the 95% prediction intervals (PI) for each prediction [45,46]. The measured coating thickness and mass were below the average predicted values, indicating less coating was deposited than expected. The elastic modulus

was also lower than the predicted value, which correlates with the lower coating thickness and mass, however the porosity and collapse stress were close to DOE predictions.

Table 3. Predicted and measured (n = 6) values for coated foam templates processed under optimized conditions for maximum mechanical properties and porosity, and minimum coating thickness and mass.

Response	Unit	Average predicted value	95% Prediction intervals (PI)	Average obtained values ± SD
Thickness per quadlayer	μm	1.16	0.45–1.87	0.81 ± 0.15
Mass per quadlayer	mg	3.22	1.66–4.78	2.72 ± 0.30
Porosity	%	87.82	81.36–91.85	88.13 ± 1.26
Elastic modulus	MPa	12.06	8.90–15.21	8.90 ± 2.21
Collapse stress	MPa	0.81	0.35–1.46	0.73 ± 0.29

The coated foam templates fabricated under the optimized conditions did not reach the targeted ranges for the cancellous bone (i.e. 0.05–0.5 GPa and 2–12 MPa for elastic modulus and collapse stress [3]) after coating deposition of 60 QL. However, with porosity of 88.1 ± 1.3%, there was sufficient pore space available to accommodate further QL deposition. Based on trends predicted by Equation 1 (with E_c = 0.7 GPa, which predicts the elastic modulus of optimized coated foams at 60 QLs), an optimized coating of 116 QL was predicted to result in a coated foam template with the minimum required elastic modulus of 50 MPa, collapse stress of 2.51 MPa, and porosity of 73.1%.

The DOE optimization did not select process conditions that resulted in the stiffest coating material (apparent elastic modulus of approximately 1.9 GPa in Figures 5a and 6a) because the

mechanical properties of coated foam templates depend on both the thickness and the elastic modulus of the coatings. In comparison, the processing conditions that resulted in the stiffest coating are predicted to achieve coated foam templates with the targeted elastic modulus of 50 MPa at a higher porosity of 83.1%, but after more deposition of 151 QL coatings and therefore longer processing times.

Cytotoxicity

Initial screening for cytotoxicity of PEI, PAA, and nanoclay indicated that PAA exhibited the lowest cytotoxicity, while PEI was highly cytotoxic (Figure S3). The outermost layer of LbL assembled coatings has been reported to dominate cell interactions and attachment [47], and so further cytotoxicity testing focused on mechanically reinforcing PEI/PAA/PEI/nanoclay coatings terminated with final capping layers of PAA. Thermal treatment (180°C for 60 min) has been reported to covalently cross-link PAA and PEI [22] and was therefore explored as a means of improving PAA capping layer stability and coating cytotoxicity. pBM-MSC cells exposed to extraction media from 10 QL DOE-optimized coated foam templates capped with PAA (10 QL optimized + PAA) exhibited ≥50% reduction in indirect cell viability at Day-14, indicating a cytotoxic effect [50] (Figure 7). The cytotoxicity of PEI (Figure S3) suggests that PEI chains may have leached into the supernatant, thereby causing this indirect cytotoxicity [17,48]. This finding is consistent with reports that LbL-assembled films prepared with weak polyelectrolytes (e.g. PEI and PAA) can swell in water and dissolve in salt solutions [49]. Without cross-linking, multilayer based coatings containing PEI can exhibit a lack of structural stability under changing physiological conditions due to the absence of chemical bonds between adjacent polyelectrolyte layers [50], and are therefore susceptible to leaching and release without a stable barrier. At Day-14, the viability of cells exposed to residual medium from optimized coated foam templates capped

with thermally treated PAA (10 QL optimized + PAA thermal) was not significantly different (p = 0.453) from uncoated counterparts, suggesting thermally cross-linked PAA capping layers were an effective physio-chemical barrier to PEI. The thermal post-treatment is expected to result in cross-linking of approximately 25% of amide groups between PAA and PEI and to enhance resistance to ionic diffusion [49]. Although the mean cell viability was higher at Day-14 for thermally treated (10 QL optimized + PAA thermal) specimens compared to specimens without thermal treatment (10 QL optimized + PAA), the difference was not significantly different (p = 0.106).

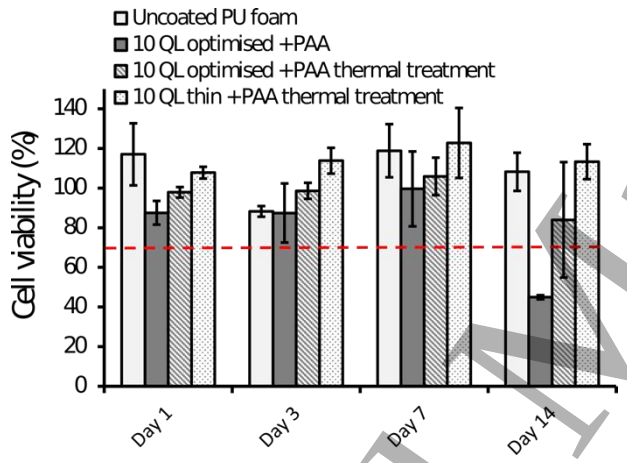

Figure 7. Viability of pBM-MSC after culture (24 h) in the supernatant conditioned with the degradation by-products from uncoated and coated foam templates deposited under varied assembly conditions (up to 14 days). Data is presented as the mean with error bars bounding one standard deviation (n = 3). The dashed line delineates 70% viability, below which is deemed cytotoxic, as designated by the ISO 10993-5 [51].

The residual product from foam templates coated under conditions associated with the thinnest coatings (PEI pH 10.5, PAA pH 8, 0 NaCl), capped with PAA, and subjected to thermal treatment (10 QL thin + PAA thermal) showed a good level of cytotoxicity with mean cell viability above 100%. Despite the higher mean viability at Day-14 for thermally treated thin coatings compared

with thermally treated optimized coatings, there was not a statistically significant difference (p = 0.288). The thinner coating is associated with less in and out diffusion during exponential LbL assembly, and therefore lower polyelectrolyte mobility. Consequently, if leaching of PEI causes reduced cell viability, then thinner coatings with lower polyelectrolyte mobility may lessen this effect.

Cell morphology is a measure of adhesion [52], and was used as a further indication of cell viability after the Day-14 incubation period (Figure 8). Following exposure to the supernatant from uncoated foam templates, the cells remained viable, spread, adhered to the surface of the well plate and exhibited a polar shape after 24 h (Figure 8a). The viability of cells exposed to the media from 10 QL optimized + PAA specimens (no thermal treatment) was relatively poor (Figure 8b). The majority of cells displayed a rounded morphology suggesting non-adherence to the well plate and apoptosis. The toxicity of media from 10 QL optimized + PAA thermal (Figure 8c) appeared lower compared to 10 QL optimized + PAA (no thermal treatment) based on cell morphology. The morphology and viability of cells exposed to media from 10 QL thin + PAA thermal specimens (Figure 8d) were comparable to the uncoated foam templates, i.e. the cells demonstrated an elongated structure and adjacent cells were joined. These observations of cell morphology were consistent with the data in Figure 7.

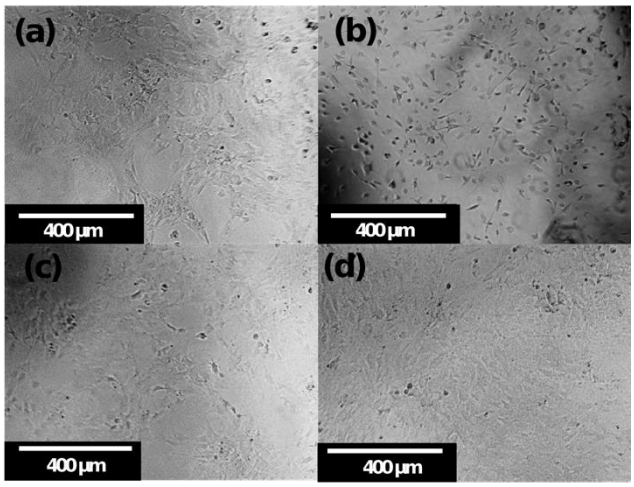

Figure 8. pBM-MSC cells in supernatant after 24 h contact with Day-14 extract from (a) an uncoated PU foam template, (b) 10 QL optimized + PAA (no thermal treatment), (c) 10 QL optimized + PAA thermal, (d) 10 QL thin + PAA thermal specimens. Images are representative of cell coverage over the entire substrate.

Deposition of multilayered coatings using LbL assembly with precise control over thickness, composition, and mechanical properties offers the opportunity for tailoring bulk properties of engineered bone scaffold materials for specific applications. The ability to decouple the bulk mechanical properties and porosity from cytotoxicity of the coating, demonstrated here, suggests that further biomedically functional constituents can be independently incorporated in order to extend achievable properties and biofunctionality. These additional functional constituents need not be limited to the surface of the coating, but can be embedded within the multilayer structure, such that multiple materials and functionalities can be usefully integrated but still separately controlled. A wide range of materials suitable for biomedical applications are compatible with LbL assembly[53]. For example, degradable layers of polylactide-co-glycolide [54], poly (β-amino ester) and poly-L-lysine [55], or others [10] could be integrated with mechanically reinforcing layers in order to control drug release and tune degradation of mechanical properties over time. Additional

functionalities that could be also incorporated include antibacterial activity and controlled cellular adhesion and proliferation (via chemical, topographical, or mechanical cues), which have also been reported using LbL assembly [10,54].

Conclusions

The influence of LbL assembly parameters on the properties of open-cell porous foam templates coated with PEI/PAA/PEI/nanoclay composites has been systematically quantified using a DOE approach. All of the response outputs investigated were predominantly affected by the pH of the PAA solution, salt concentration and the interaction between these two factors. Although cyclic mechanical deformation was not a dominant factor for the response outputs tested, it was specified as part of the optimized conditions and therefore may affect LbL assembly as hypothesized—confirmation of this requires further investigation. In most cases, the mechanical properties of coated foams correlated directly with the factors affecting the thickness of the coatings, with thicker coatings leading to higher mechanical properties. However, high levels of salt concentration (1 M NaCl) were associated with lower mechanical properties at similar thicknesses, which is consistent with lower elastic moduli of the coating materials. Cytotoxicity studies indicated that sub-surface PEI layers did not induce a cytotoxic response after 14 days when coatings were capped with PAA and thermally cross-linked, suggesting suitability for engineered bone tissue scaffold applications. Scaffolds coated with 116 or more QLs were predicted to exhibit mechanical strength (2.51 MPa) and stiffness (50 MPa) in the same range as cancellous bone and with suitably high porosity (73.1% predicted under optimized conditions). Further work is necessary to experimentally confirm these predictions, characterize mechanical performance under more representative physiological conditions, confirm the cytotoxicity over extended periods and

for thicker coatings >10 QL, investigate the mechanical effects of thermal crosslinking, and to incorporate additional functional constituents.

Supporting Information

The supporting information includes individual assembly conditions, results of each of the experimental run and the characterization of cytotoxicity of the individual layers of PEI, PAA and nanoclay.

Corresponding Author

* E-mail: A.R.Hamilton@soton.ac.uk

Present Addresses

†If an author's address is different than the one given in the affiliation line, this information may be included here.

Funding Sources

The research leading to these results has received funding from the People Programme (Marie Curie Actions) of the European Union's Seventh Framework Programme FP7/2007-2013/ under REA grant agreement n° [631079] "NanoGrow", awarded to A.R.H. M.Z. and J.A. were supported by Research Studentships from the Department for Employment and Learning, Northern Ireland.

References

1. Campana, V., Milano, G., Pagano, E., Barba, M., Cicione,C., Salonna, G., Lattanzi, W. and Logroscino, G. Bone substitutes in orthopaedic surgery: from basic science to clinical practice. J. Mater. Sci. Mater. Med. **25**, 2445–2461 (2014).

2. Giannoudis, P. V., Dinopoulos, H. and Tsiridis, E. Bone substitutes: An update. Injury **36**, 20–27 (2005).

3. Hutmacher, D. W., Schantz, J. T., Lam, C. X. F., Tan, K. C. and Lim, T. C. State of the art and future directions of scaffold-based bone engineering from a biomaterials perspective. J. Tissue Eng. Regen. Med. **1**, 245–260 (2007).

4. Bose, S., Vahabzadeh, S. and Bandyopadhyay, A. Bone tissue engineering using 3D printing. Mater. Today **16**, 496–504 (2013).

5. Fedorovich, N. E., Alblas, J., Hennink, W. E., Öner, F. C. and Dhert, W. J. A. Organ printing: the future of bone regeneration? Trends Biotechnol. **29**, 601–606 (2011).

6. Doyle, H., Lohfeld, S. and McHugh, P. Predicting the Elastic Properties of Selective Laser Sintered PCL/β-TCP Bone Scaffold Materials Using Computational Modelling. Ann. Biomed. Eng. **42**, 661–677 (2014).

7. Bose, S., Roy, M. and Bandyopadhyay, A. Recent advances in bone tissue engineering scaffolds. Trends Biotechnol. **30**, 546–554 (2012).

8. Gil, E. S., Kluge, J. A., Rockwood, D. N., Rajkhowa, R., Wang, L., Wang X. and Kaplan, D. L.Mechanical improvements to reinforced porous silk scaffolds. J. Biomed. Mater. Res. Part A **99A**, 16–28 (2011).

9. Xiao, F.-X., Pagliaro, M., Xu, Y.-J. and Liu, B. Layer-by-layer assembly of versatile nanoarchitectures with diverse dimensionality: a new perspective for rational construction of multilayer assemblies. Chem. Soc. Rev. **45**, 3088–121 (2016).

10. Boudou, T., Crouzier, T., Ren, K., Blin, G. and Picart, C. Multiple Functionalities of Polyelectrolyte Multilayer Films: New Biomedical Applications. Adv. Mater. **22**, 441–467 (2010).

11. Podsiadlo, P., Michel, M., Lee, J., Verploegen, E., Wong Shi Kam, N., Ball, V., Lee, J., Qi, Y., John Hart, A., Hammond, P. T. and Kotov, N. A. Exponential Growth of LBL Films with Incorporated Inorganic Sheets. Nano Lett. **8**, 1762–1770 (2008).

12. Ziminska, M., Dunne, N. and Hamilton, A. R. Porous Materials with Tunable Structure and Mechanical Properties via Templated Layer-by-Layer Assembly. ACS Appl. Mater. Interfaces **8**, 21968–21973 (2016).

13. Dubas, S. T. and Schlenoff, J. B. Swelling and Smoothing of Polyelectrolyte Multilayers by Salt. Langmuir **17**, 7725–7727 (2001).

14. Picart, C., Mutterer, J., Mutterer, Richert, L., Luo, Y., Prestwich, G. D., Schaaf, P., Voegel, J.-C. and Lavalle, P. Molecular basis for the explanation of the exponential growth of polyelectrolyte multilayers. Proc. Natl. Acad. Sci. U. S. A. **99**, 12531–5 (2002).

15. Liu, X., Zhou, L., Liu, F., Ji, M., Tang, W., Pang, M. and Sun, J. Exponential growth of layer-by-layer assembled coatings with well-dispersed ultrafine nanofillers: a facile route to scratch-resistant and transparent hybrid coatings. J. Mater. Chem. **20**, 7721 (2010).

16. Lavalle, P., Picart, C., Mutterer, J., Gergely, C., Reiss, H., Voegel, J.-C., Senger, B. and Schaaf, P.Modeling the Buildup of Polyelectrolyte Multilayer Films Having Exponential Growth. J. Phys. Chem. B **108**, 635–648 (2004).

17. Fu, J. Ji, J., Shen, L., Külle, A., Rosenhahn, A., Shen, J. and Grunze. M. pH-Amplified Exponential Growth Multilayers: A Facile Method to Develop Hierarchical Micro- and Nanostructured Surfaces. Langmuir **25**, 672–675 (2009).

18. Yang, Y.-H., Malek, F. A. and Grunlan, J. C. Influence of Deposition Time on Layer-by-Layer Growth of Clay-Based Thin Films. Ind. Eng. Chem. Res. **49**, 8501–8509 (2010).

19. Kinoshita, Y. and Maeda, H. Recent Developments of Functional Scaffolds for Craniomaxillofacial Bone Tissue Engineering Applications. Sci. World J. 1–21 (2013).

20. Patel, P.S.D., Shepherd, D.E. and Hukins, D.W. Compressive properties of commercially available polyurethane foams as mechanical models for osteoporotic human cancellous bone. BMC Musculoskelet. Disord. **9**, 137-144 (2008).

21 Jiang, H., Sitoci-Ficici, K.H., Reinshagen, C., Molcanyi, M., Zivcak, J., Hudak, R., Laube, T., Schnabelrauch, M., Weisser, J., Schäfer, U., Pinzer, T, Schackert12, G., Zhang, X., Wähler, M., Brautferger, U. and Rieger, B. Adjustable Polyurethane Foam as Filling Material for a Novel Spondyloplasty: Biomechanics and Biocompatibility. World Neurosurg. **112**, 848–858 (2018).

22 Yang, Y.-H., Bolling, L., Haile, M. and Grunlan, J. C. Improving oxygen barrier and reducing moisture sensitivity of weak polyelectrolyte multilayer thin films with crosslinking. RSC Adv. **2**, 12355 (2012).

23. May, G. S. and Spanos, C. J. Statistical Experimental Design. in Fundamentals of Semiconductor Manufacturing and Process Control 228–271 (John Wiley & Sons, 2006).

24. Jaber, J. A. and Schlenoff, J. B. Recent developments in the properties and applications of polyelectrolyte multilayers. Curr. Opin. Colloid Interface Sci. **11**, 324–329 (2006).

25. Gong, X. and Gao, C. Influence of salt on assembly and compression of PDADMAC/PSSMA polyelectrolyte multilayers. Phys. Chem. Chem. Phys. **11**, 11577 (2009).

26. Albro, M. B., Chahine, N. O., Li, R. Yeager, K., Hung, C. T. and Ateshian G. A. Dynamic loading of deformable porous media can induce active solute transport. J. Biomech. **41**, 3152–7 (2008).

27. Michel, M., Toniazzo, V., Ruch, D. and Ball, V. Deposition Mechanisms in Layer-by-Layer or Step-by-Step Deposition Methods: From Elastic and Impermeable Films to Soft Membranes with Ion Exchange Properties. ISRN Mater. Sci. **3**, 701695 (2012).

28. Mertz, D., Hemmerlé, J., Mutterer, J., Ollivier, S., Voegel, J.-C., Schaaf, P. and Lavalle, P. Mechanically Responding Nanovalves Based on Polyelectrolyte Multilayers. Nano Lett. **7**, 657-662 (2007).

29. Montgomery, D. C. Chapter 6: The 2k Factorial Design. in Design and Analysis of Experiments 233–292 (John Wiley & Sons, 2012).

30. Partee, B., Hollister, S. J. and Das, S. Selective Laser Sintering Process Optimization for Layered Manufacturing of CAPA® 6501 Polycaprolactone Bone Tissue Engineering Scaffolds. J. Manuf. Sci. Eng. **128**, 531–540 (2005).

31. Bouxsein, M.L., Boyd, S.K., Christiansen, B.A., Guldberg, R.E., Jepsen, K.L. and Müller, R. Guidelines for assessment of bone microstructure in rodents using micro-computed tomography. J. Bone Miner. Res. **25**, 1468–1486 (2010).

32. West Conshohocken, PA: ASTM International. ASTM Standards D1621-10. Standard Test Method for Compressive Properties of Rigid Cellular Plastics. (2010).

33. O'Hara, R.M., Dunne, N.J., Orr, J.F., Buchanan, F.J., Wilcox, R.K. and Barton, D.C.Optimisation of the mechanical and handling properties of an injectable calcium phosphate cement. J. Mater. Sci. Mater. Med. **21**, 2299–2305 (2010).

34. Strober, W. Monitoring Cell Growth. in Current Protocols in Immunology (eds. Coligan, J. E., Bierer, B. E., Margulies, D. H., Shevach, E. M. & Strober, W.) (John Wiley & Sons, Inc., 2001).

35. Burke, S. E. and Barrett, C. J. Acid−Base Equilibria of Weak Polyelectrolytes in Multilayer Thin Films. Langmuir **19**, 3297-3303 (2003).

36. Wang, W., Xu, Y., Backes, S., Li, A., Micciulla, S., Basak Kayitmazer, A., Li, L., Guo, X. and von Klitzing, R. Construction of Compact Polyelectrolyte Multilayers Inspired by Marine Mussel: Effects of Salt Concentration and pH As Observed by QCM-D and AFM. Langmuir **32**, 3365–3374 (2016).

37. Yang, Y.-H., Haile, M., Park, Y. T., Malek, F. A. and Grunlan, J. C. Super Gas Barrier of All-Polymer Multilayer Thin Films. Macromolecules **44**, 1450–1459 (2011).

38. Han, B., Chery, D. R., Yin, J., Lu, X. L., Lee, D. and Han, L. Nanomechanics of layer-by-layer polyelectrolyte complexes: a manifestation of ionic cross-links and fixed charges. Soft Matter **12**, 1158–1169 (2016).

39. Mjahed, H., Voegel, J-C., Senger, B., Chassepot, A., Rameau, A. Ball, V., Schaaf, P. and Boulmedaisc F. Restructuring of exponentially growing polyelectrolyte multilayer films induced by salt concentration variations after film deposition. J. Mater. Chem. **21**, 8416–8421 (2011).

40. Andreas Fery, Björn Schöler, Thierry Cassagneau, and Caruso, F. Nanoporous Thin Films Formed by Salt-Induced Structural Changes in Multilayers of Poly(acrylic acid) and Poly(allylamine). Langmuir **17**, 3779-3783 (2001).

41. Cho, C., Wallace, K. L., Hagen, D. A., Stevens, B., Regev, O. and Grunlan, J. C. Nanobrick wall multilayer thin films grown faster and stronger using electrophoretic deposition *Nanotechnology*, **26**, 185703 (2015).

42. Gibson, L. J. and Ashby, M. F. Cellular Solids: Structure and properties. (Cambridge University Press, 1997).

43. Cheng, N.G., Gopinath, A., Wang, L., Iagnemma, K. and Hosoi, A.E. Thermally Tunable, Self-Healing Composites for Soft Robotic Applications. *Macromol. Mater. Eng.* **299**, 1279-1284 (2014).

44. Gunatillake, P. A., Meijs, G. F., McCarthy, S. J. and Sherriff, N. Polyurethane elastomers with low modulus and hardness based on novel copolyether macrodiols. J. Appl. Polym. Sci. **63**, 1373–1384 (1997).

45. Kraber, S. How to get started with Design-Expert software. (2013).

46. Kraber, S., Whitcomb, S. & Anderson, M. Handbook for Experimenters. Version 06.8. (2016).

47. Müller, M., Rieser, T., Dubin, P. L. and Lunkwitz, K. Selective Interaction Between Proteins and the Outermost Surface of Polyelectrolyte Multilayers: Influence of the Polyanion Type, pH and Salt. Macromol. Rapid Commun. **22**, 390–395 (2001).

48. Martinez, J. S., Keller, T. C. S. and Schlenoff, J. B. Cytotoxicity of Free versus Multilayered Polyelectrolytes. Biomacromolecules **12**, 4063–4070 (2011).

49. Lin, K., Gu, Y., Zhang, H., Qiang, Z., Vogt, B.D. and Zacharia, N.S. Accelerated Amidization of Branched Poly(ethylenimine)/Poly(acrylic acid) Multilayer Films by Microwave Heating. Langmuir **32**, 9118–9125 (2016).

50. He, T. and Chan, V. Covalent layer-by-layer assembly of polyethyleneimine multilayer for antibacterial applications. J. Biomed. Mater. Res. Part A **95A**, 454–464 (2010).

51. ISO. ISO 10993-5:2009. Biological evaluation of medium devices - Part 5: Tests for in vitro cytotoxicity. (2009).

52. Kirchhof, K., Hristova, K., Krasteva, N., Altankov, G. and Groth, T. Multilayer coatings on biomaterials for control of MG-63 osteoblast adhesion and growth. J. Mater. Sci. Mater. Med. 20, 897–907 (2009).

53. Costa, R. R., and Mano, J. F. Polyelectrolyte Multilayered Assemblies in Biomedical Technologies. Chem Soc Rev **43**, 3453–3479 (2014).

54. Gentile, P., Frongia, M.E., Cardellach, M., Miller, C.A., Stafford, G.P., Leggett, G.J. and Hatton, P.V. "Functionalised nanoscale coatings using layer-by-layer assembly for imparting antibacterial properties to polylactide-co-glycolide surfaces," Acta Biomater. **21**, 35–43 (2015).

55. D. Choi and J. Hong, "Layer-by-layer assembly of multilayer films for controlled drug release," Arch. Pharm. Res. **37**, 79–87 (2014).

Table of Contents graphic